#### Log Number: 117

# VOID FRACTION EVOLUTION IN SUBCOOLED FLOW BOILING UNDER LOW-PRESSURE AND LOW-FLOWRATE CONDITION

# T. Okawa, Y. Yamagoe and R. Ahmadi

Department of Mechanical Engineering, Osaka University, Osaka, Japan t-okawa@mech.eng.osaka-u.ac.jp, yamagoe@ihmt.mech.eng.osaka-u.ac.jp, ahmadi@ihmt.mech.eng.osaka-u.ac.jp

#### Abstract

Visualization of bubble behavior in water subcooled flow boiling was carried out to investigate the triggering mechanism of the net vapor generation under a low-pressure and low-flowrate condition. Flow direction was vertical upward and a hydrophilic surface was used as the heated surface. In the experiments under high liquid subcooling, bubbles were lifted off the heated surface immediately after the nucleation and collapsed in the subcooled bulk liquid. Since the condensation rate was nearly equal to the vaporization rate, the vapor void fraction did not increase significantly. When the liquid subcooling was low enough, bubble coalescence took place to produce large bubbles sliding up the vertical heated surface. It was considered that the large sliding bubbles mitigated the condensation to contribute to a rapid increase in the vapor void fraction with an increase in the thermal-equilibrium quality.

### 1. Introduction

Vapor void fraction in subcooled flow boiling region is an important parameter influencing the fuel burnup and the inception of two-phase flow instabilities in nuclear power plants. In particular, a high-power-density core tends to be adopted to further enhance economic efficiency in recent advanced light water reactors [1–4]. In industrial plants that use a forced convective boiling heat transfer, however, increased power density generally leads to the reduction of the margin to the onset of unanticipated flow instability. Accurate prediction of the void fraction in subcooled boiling region is hence of increasing importance to surely avoid the flow instabilities.

From the standpoint of the axial evolution of the vapor void fraction, the subcooled boiling region can be divided into the two regions [5]. In the upstream region of high liquid subcooling, sufficiently high wall superheat permits the formation of bubbles at the nucleation cavities but the void fraction is kept low. Only in the downstream region of low liquid subcooling, a rapid increase in the vapor void fraction with an increase in the thermal equilibrium quality can be observed. Since the void fraction in the upstream region is usually neglected, the boundary between the two regions is regarded as the point of net vapor generation (PNVG). It is known that accurate determination of the PNVG is of essential importance in predicting the axial void fraction evolution in the subcooled boiling region [6]. Because of the practical importance of PNVG, several empirical correlations have been developed [7, 8]. Although these correlations are useful to predict the PNVG in reasonably wide range of thermal-hydraulic conditions, the triggering mechanism of NVG has not been elucidated. Levy postulated that the bubble departure from the nucleation site triggers the NVG, and developed a mechanistic correlation for the PNVG [9]. Several investigators however observed that bubbles did not stay at the nucleation

Log Number: 117

cavities even under the conditions close to the onset of nucleate boiling (ONB) [10–12]. It is therefore considered that the bubble departure model does not apply to the experimental conditions tested in these studies.

The main objective of this work is to investigate the triggering mechanism of the NVG in water subcooled flow boiling. It is considered that the mechanism may be dependent on the thermal-hydraulic conditions including the system pressure, mass flux and the heat flux. In fact, Saha and Zuber suggested that the NVG is caused by different mechanisms in the thermally controlled region at low Peclet numbers and the hydrodynamically controlled region at high Peclet numbers [7]. In the present work, however, the experiments are conducted under a low-pressure and low-flowrate condition as the first step. Furthermore, Levy postulated that the surface tension force is the major component to hold the bubbles to the heated surface [9]. Therefore, the contact angle of the heated surface would also be influential in the PNVG. Since the contact angle is considered to be small in the nuclear reactor core due to the high-temperature and radiation environments [13, 14], the surface of small contact angle is used as the heated surface in the present experiments.

## 2. Experimental description

Figure 1a shows the flow loop used in the present experiments. A canned motor pump was used to drive the working fluid through the loop. The total mass flow rate was measured using a turbine flow meter. The fluid was preheated using two 5 kW sheath heaters to set the inlet subcooling, then injected to a test section through an inlet header. After exiting the test section, the steam-water mixture entered the separator through an outlet header. Vapor phase was then sent to a condenser. The heat transfer rate in the condenser was controlled to maintain the system pressure. The fluid temperature was reduced at the cooling section before returning to the circulation pump. Temperatures and pressures were measured using type-K thermocouples and pressure transducers, respectively. The measurement points are shown schematically in Fig. 1a.

Depicted in Fig. 1b is a schematic diagram of the test section. A main body of the test section was made of SUS316 stainless steel. A copper block containing two 1.2 kW cartridge heaters was set on the main body to construct the flow channel. The flow area was rectangular in shape of 10 x 20 mm. As delineated in the top view in Fig. 1b, the copper block was covered by the stainless steel jacket. The end face of the copper block of 10 mm in width was regarded as the heated surface. The present heated surface was rather hydrophilic as shown in Fig. 2 and its average contact angle was 12°. The copper block and the jacket were connected smoothly by means of electron beam welding to avoid significant boiling in the connecting region. The total heated length was 400 mm. The test section had two measuring sections at 100 and 300 mm from the bottom of the heated section. At each measuring section, three thermocouples were embedded in the copper block to determine the wall superheat. The fluid temperature and the void fraction could be measured using a type-K thermocouple and an optical void probe, respectively. These probes were traversed using micrometers to measure the lateral distributions. In addition, two sets of glass windows were mounted at the measuring sections for visual observation of bubbles using a high-speed camera and a metal halide lamp. The spatial resolution and the frame rate were set to 0.022 mm/pixel and 6000 frames/s, respectively, and the region of about 10 x 10 mm was imaged.

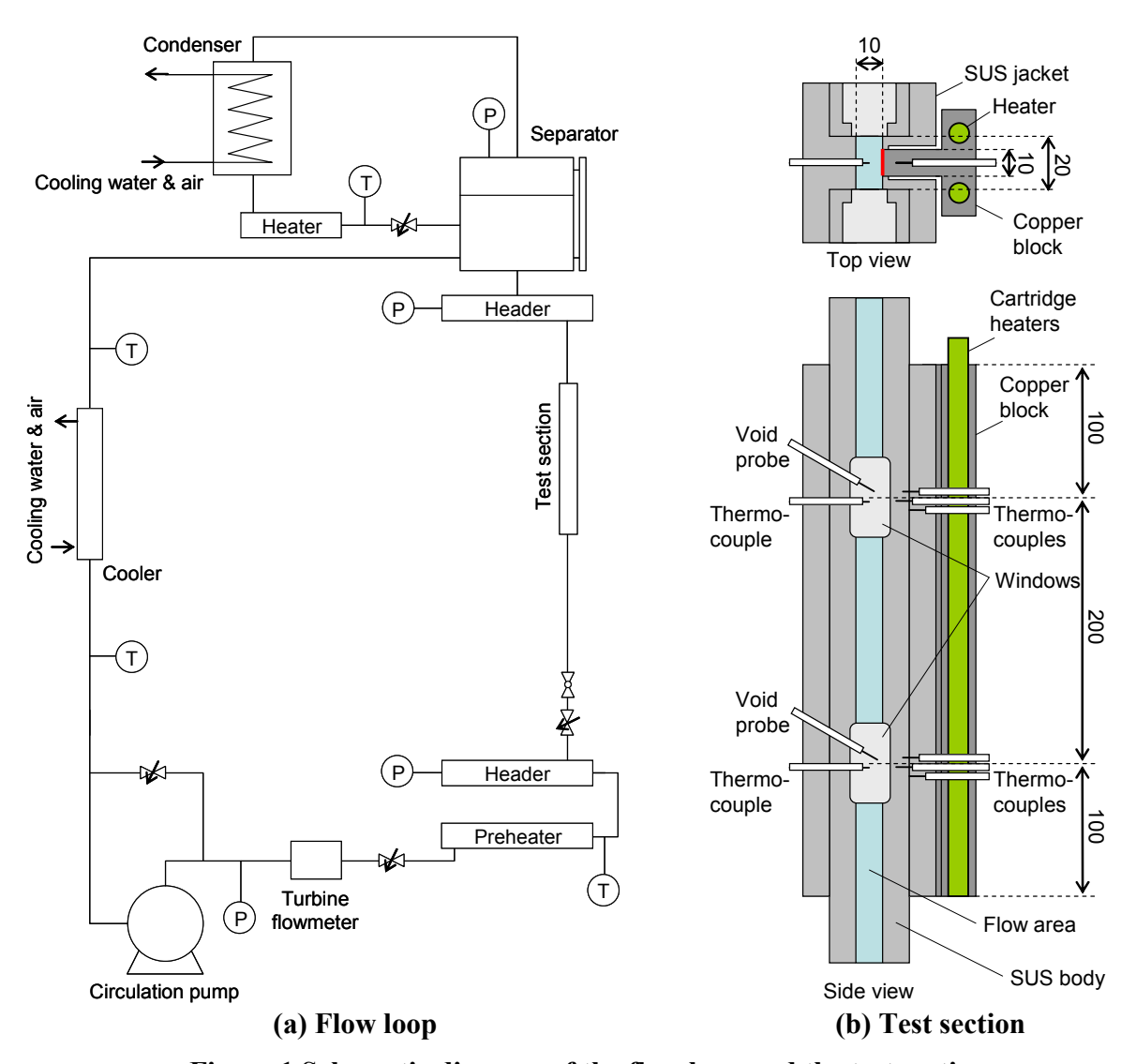


Figure 1 Schematic diagram of the flow loop and the test section.

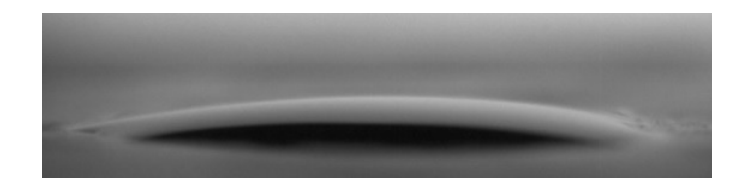


Figure 2 Image of a water droplet placed on the heated surface.

Filtrated and deionized tap water was used as a working fluid. It was kept boiling for about an hour in a storage tank containing a sheath heater for degassing. The loop was vacuumed prior to the experiment to supply the working fluid from the storage tank by means of pressure

difference. In the present experiments, measurements were performed at the upper measuring section 300 mm from the bottom of the heated section after the steady state was reached. Main experimental conditions are listed in Table 1. Here, Run No. 1 corresponds to the ONB. The mass flux G and the heat flux  $q_w$  were set to 605–615 kg/m²s and 300 kW/m², respectively, and the inlet fluid temperature  $T_{IN}$  was changed parametrically. As shown in Table 1, the local subcooling at the upper measuring section  $\Delta T_{SUB}$  decreased and the thermal equilibrium quality  $x_{eq}$  at the measuring section increased gradually with an increase in  $T_{IN}$ . In the present experiment, the test section pressure P increased with an increase in  $T_{IN}$  mainly due to an increase in the frictional pressure loss.

Run	G (kg/m <sup>2</sup> s)	$q_w (kW/m^2)$	<i>T<sub>IN</sub></i> (C)	$\Delta T_{SUB}$ (K)	P (kPa)	$T_{SAT}$ (C)	$x_{eq}$	Pe	Nu
1	615	300	58	30.8	66	88	-0.326	51536	195
2	611	300	70	22.6	79	92	-0.224	50909	260
3	612	300	80	16.4	92	97	-0.151	50851	361
4	609	300	90	8.5	100	100	-0.068	50538	693
5	605	300	95	5.9	110	102	-0.041	50195	999
6	605	300	100	4.2	121	105	-0.023	50148	1419

Table 1 Main experimental conditions.

# 3. Experimental results

### 3.1 Bubble behavior at ONB

Typical bubble behavior observed at the ONB (Run No. 1) is displayed in Fig. 3. In this case, only one nucleation site was activated and five bubbles were produced within 50 ms. The size of bubbles ranged from 0.7 to 1.4 mm, but all the five bubbles behaved as shown in Fig. 3. The time-evolutions of the dimensions of the bubble depicted in Fig. 3 are displayed in Fig. 4. Here,  $d_{BX}$  and  $d_{BY}$  are the maximum bubble dimensions in the horizontal and vertical directions, respectively, and  $d_B$  is the arithmetic average of  $d_{BX}$  and  $d_{BY}$ . It can be seen that  $d_B$  increased rapidly in the initial stage but the growth rate decreased gradually since the bubble was exposed to the subcooled liquid. It may be interesting to note that although  $d_B$  decreased rapidly after the lift-off from the heated surface, the reduction of  $d_B$  already commenced before the detachment from the heated surface since the condensation rate around the bubble overcame the evaporation rate at the base of the bubble. It can also be seen that the bubble was flattened along the heated surface in the initial stage  $(d_{BY} > d_{BX})$ , but it was rounded gradually  $(d_{BY} \approx d_{BX})$  and was elongated in the perpendicular direction to the surface at the moment of lift-off ( $d_{BY} < d_{BX}$ ). It is hence considered that the local liquid flow formed around the bubble due to time-evolutions of the size and shape of the bubble contributed to lift the bubble off the heated surface as discussed by Okawa et al. [15]. The bubble behavior depicted in Fig. 3 indicates that the surface tension force to hold the bubble at the nucleation site was not sufficient to prevent the bubble lift-off even at the ONB under the low-pressure, low-flowrate and low-contact angle condition tested in the present work.

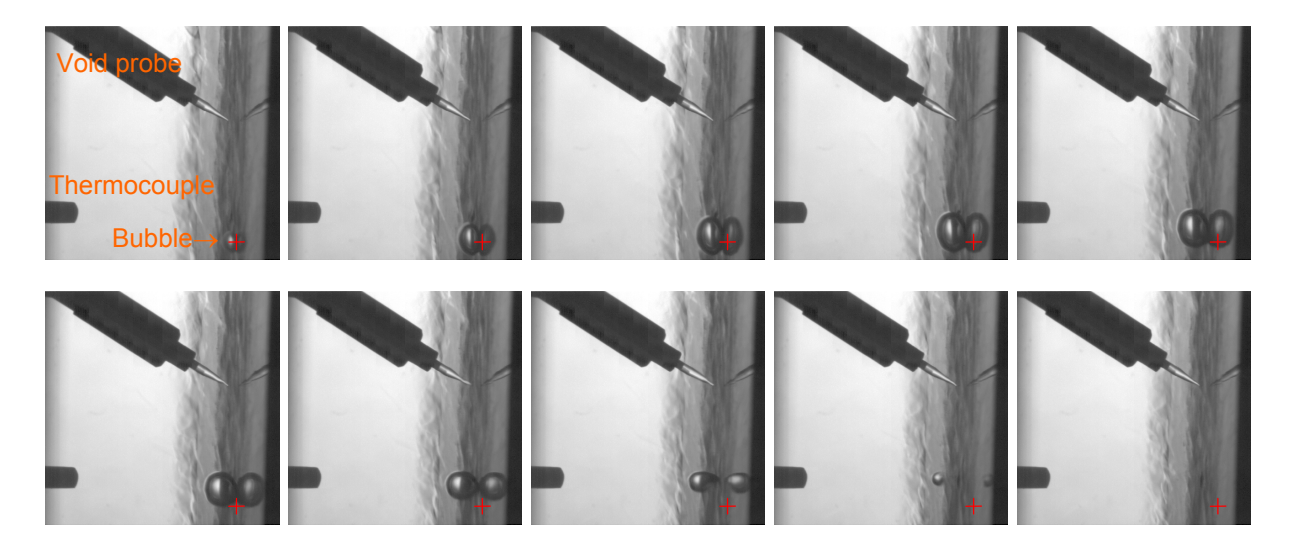


Figure 3 Bubble behavior observed at the ONB (Run No. 1; time interval = 0.5 ms).

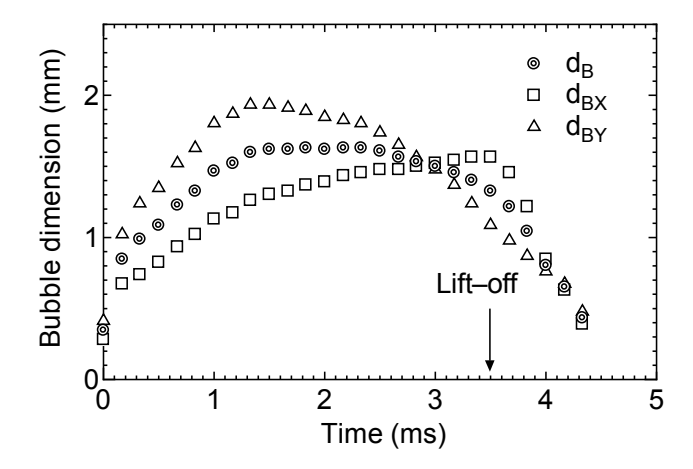


Figure 4 Time-evolutions of dimensions of the bubble depicted in Fig. 3.

# 3.2 Void fraction evolution with a decrease in the liquid subcooling

In the experiments at low inlet temperatures (Run Nos. 1–3), bubbles were usually collapsed near the nucleation sites at which they were produced (see Fig. 3). In consequence, the void fraction measured by the void probe was influenced by the relative positions of the probe and the active nucleation sites. For example, in the case shown in Fig. 3, one nucleation site was activated but the void fraction measured by the probe was zero since no bubble hit the probe. Therefore, the void fraction within the visualization region was measured by means of image analysis. Examples of the snapshots used in the image analysis are depicted in Fig. 5. To obtain lateral distributions of the void fraction, the camera was set parallel to the heated surface. Since the instantaneous void fraction was different between the snapshots particularly in the low inlet temperature experiments, 10-25 snapshots were used depending on  $T_{IN}$ . In the experiment of the highest inlet temperature (Run No. 6), however, the void fraction measurement by the image analysis was not possible because of significant overlapping of bubbles. The void fraction

distributions were hence measured using the void probe in this experimental condition. The measured void fraction distributions are displayed in Fig. 6a. Here, y is the distance from the heated surface. It can be seen that the peak void fraction and the thickness of the region in which the void fraction was positive increased with a decrease in the liquid subcooling. The local void fractions shown in Fig. 6a were integrated in the y-direction to derive the time-averaged void fraction within the visualization window  $\alpha$ . The calculated values of  $\alpha$  are plotted against  $x_{eq}$  in Fig. 6b. It can be seen that  $\alpha$  was kept less than 0.01 in Run Nos. 1–3 but it increased rapidly with an increase in  $x_{eq}$  in Run Nos. 4–6.

In the present experiments, the ranges of the Peclet number  $Pe = GD_hc_{pl}/k_l$  and the Nusselt number  $Nu = q_wD_h/k_l\Delta T_{SUB}$  were within 50148–51536 and 195–1419, respectively (see Table 1). Saha and Zuber defined the boundary between the thermally and hydrodynamically controlled regions by Pe = 70000 [7], and consequently the present experimental conditions belonged to the thermally controlled region in their notation. In this region, the PNVG is correlated by Nu = 455 that corresponds to  $x_{eq} = -0.13$  in the present experiment. From the result shown in Fig. 6b, it is considered that the onset of NVG in the present experiment agreed with the correlation by Saha and Zuber fairly well.

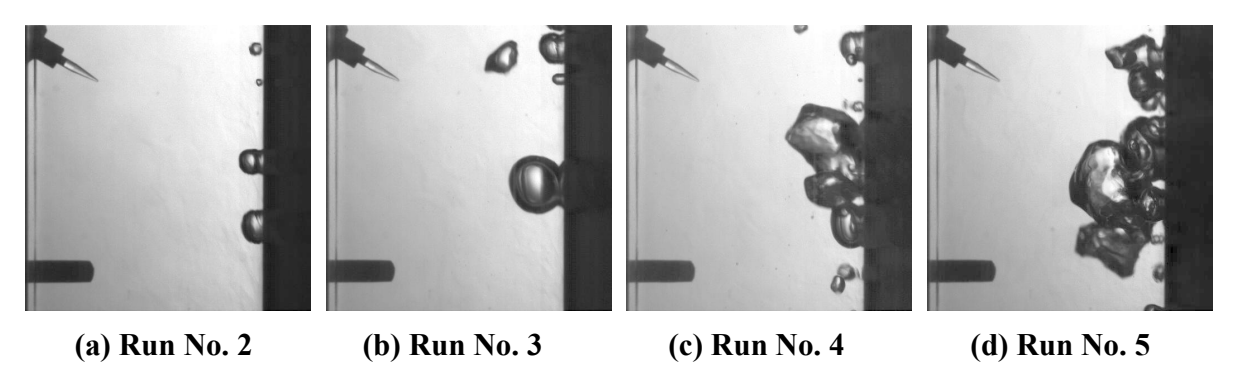
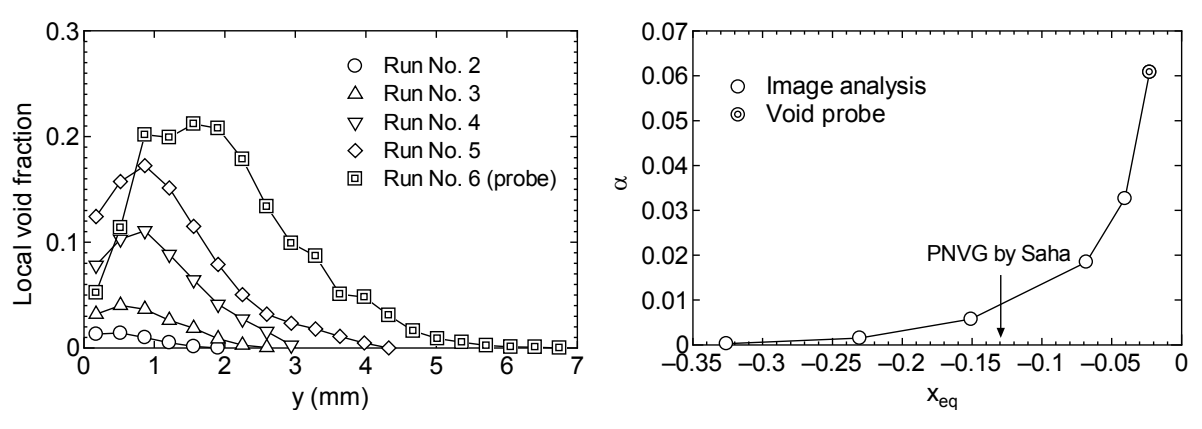


Figure 5 Examples of snapshots used in the void fraction measurements.



(a) Lateral distributions of local void fraction (b) Dependence of the void fraction on  $x_{eq}$ Figure 6 Distributions of vapor void fraction.

## 4. Discussion

In the present experiments, bubbles were detached from the heated surface and propelled into the subcooled bulk liquid even at the ONB as shown in Fig. 3. Therefore, neither the bubble departure from the nucleation site nor the bubble lift-off from the heated surface is considered to be the triggering mechanism of the NVG. The continuity equation of the vapor phase in the steady state is given by

$$\frac{d}{dz}(\alpha \rho_g u_g) = \Gamma_V - \Gamma_C \tag{1}$$

where z is the axial coordinate,  $\rho$  is the density, u is the velocity in the vertical direction,  $\Gamma_V$  is the vaporization rate,  $\Gamma_C$  is the condensation rate, and the subscript g denotes the vapor phase. If  $\rho_g$  and  $u_g$  are assumed to be constant for simplicity and the condensation heat transfer coefficient is denoted by  $h_C$ , the above equation is reduced to

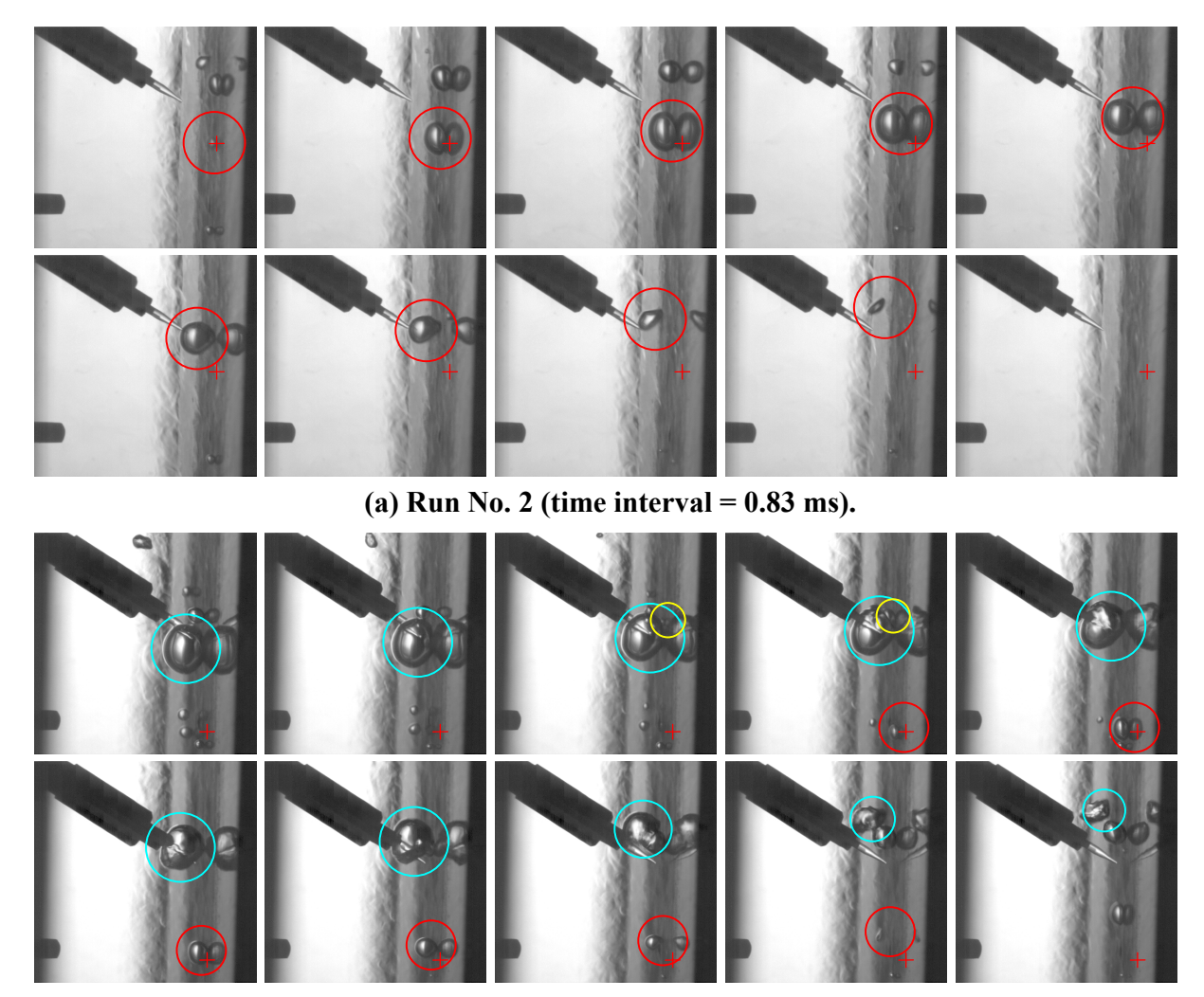
$$\frac{d\alpha}{dx_e} = \frac{GA\Delta h_V}{q_w W_h \rho_e u_g} (\Gamma_V - \Gamma_C) = \frac{GA\Delta h_V}{q_w W_h \rho_e u_g} \left( \Gamma_V - \frac{6h_C \Delta T_{SUB}^b}{\Delta h_V d_{SM}} \alpha \right)$$
(2)

where A is the cross-sectional area of the flow channel,  $\Delta h_V$  is the latent heat of vaporization,  $W_h$  is the width of the heated surface,  $d_{SM}$  is the Sauter mean bubble diameter, and the superscript b denotes the reference value for bubble; the independent variable z in Eq. 1 is replaced by  $x_{eq}$  in Eq. 2. Equation 2 indicates that the difference between  $\Gamma_V$  and  $\Gamma_C$  is of importance for  $\alpha$  to increase with an increase in  $x_{eq}$ .

As shown in Fig. 3, all the bubbles disappeared in close proximity to the nucleation site due to rapid condensation in Run No. 1. Therefore,  $\Gamma_V \approx \Gamma_C$  holds and a rapid increase in  $\alpha$  with  $x_{eq}$  is not permitted. Important bubble behavior observed in Run Nos. 2–6 is displayed in Figs. 7a–e, respectively. In Run Nos. 2 and 3, most bubbles behaved like those in Run No. 1 (see the bubbles surrounded by the red circles in Figs. 7a and b). Although bubble coalescence was observed several times in Run No. 3 (see the bubbles surrounded by the light blue and yellow circles in Fig. 7b), the coalesced bubbles also moved away from the wall and collapsed in the subcooled bulk liquid. Since the bubble behavior was essentially the same, a slight increase in  $\alpha$  with  $x_{eq}$  in Run Nos. 1–3 may simply be attributed to the reductions of the single-phase heat transfer and the condensation rate caused by a decrease in  $\Delta T_{SUB}$ .

An interesting observation was made in Run No. 4. The bubble surrounded by the light blue circles coalesced with the two other bubbles surrounded by the green and yellow circles. The coalescences contributed to an increase in the bubble size and mitigated the unidirectional bubble migration away from the wall. As a result, a large bubble was created as indicted by the red circle in the last photo in Fig. 7c. A drastic change of the bubble behavior was observed in Run No. 5. In this case, many large bubbles came from the bottom of the visualization window and captured the new bubbles produced in the visualization region. One large bubble is indicated by the light blue arrows in Fig. 7d as an example. It can be seen that the large bubbles rose up in the high-temperature region near the heated surface. Therefore, a continuous reduction of the bubble size did not take place. The shear-induced lift force was considered to be the main force

to push the bubbles against the wall. Since the large bubbles rose up faster than other bubbles, they frequently collided with other small bubbles (see Fig. 7d; here, different bubbles are indicated by the arrows of different color). Since the small bubbles were usually absorbed in the large bubble after the collision, they were not propelled into the bulk liquid. If bubbles coalesce into a large sliding bubble, the bubble life-time is significantly be elongated. Furthermore, since the large sliding bubbles repeat the coalescence with small bubbles, they also contribute to the elongation of the life-time of other bubbles. It may also be possible that the large sliding bubbles contribute to enhancing the vaporization since a thin liquid film is formed between the bubble and the wall. Figure 7e indicates that larger portion of the heated surface was covered by the large sliding bubbles in Run No. 6. It is therefore expected that the mitigation of the condensation and the enhancement of the vaporization caused by the large sliding bubbles were further pronounced. It is noted that in all the experiments, bubbles were lifted-off the wall to collapse in the subcooled liquid unless they coalesced with other bubbles. It is hence considered that the bubble coalescence followed by the formation of large sliding bubbles played an important role to initiate a rapid increase in  $\alpha$  with  $x_{eq}$  under the present experimental condition.



(b) Run No. 3 (time interval = 0.67 ms).

Figure 7 Bubble behavior observed in Run Nos. 2–6.

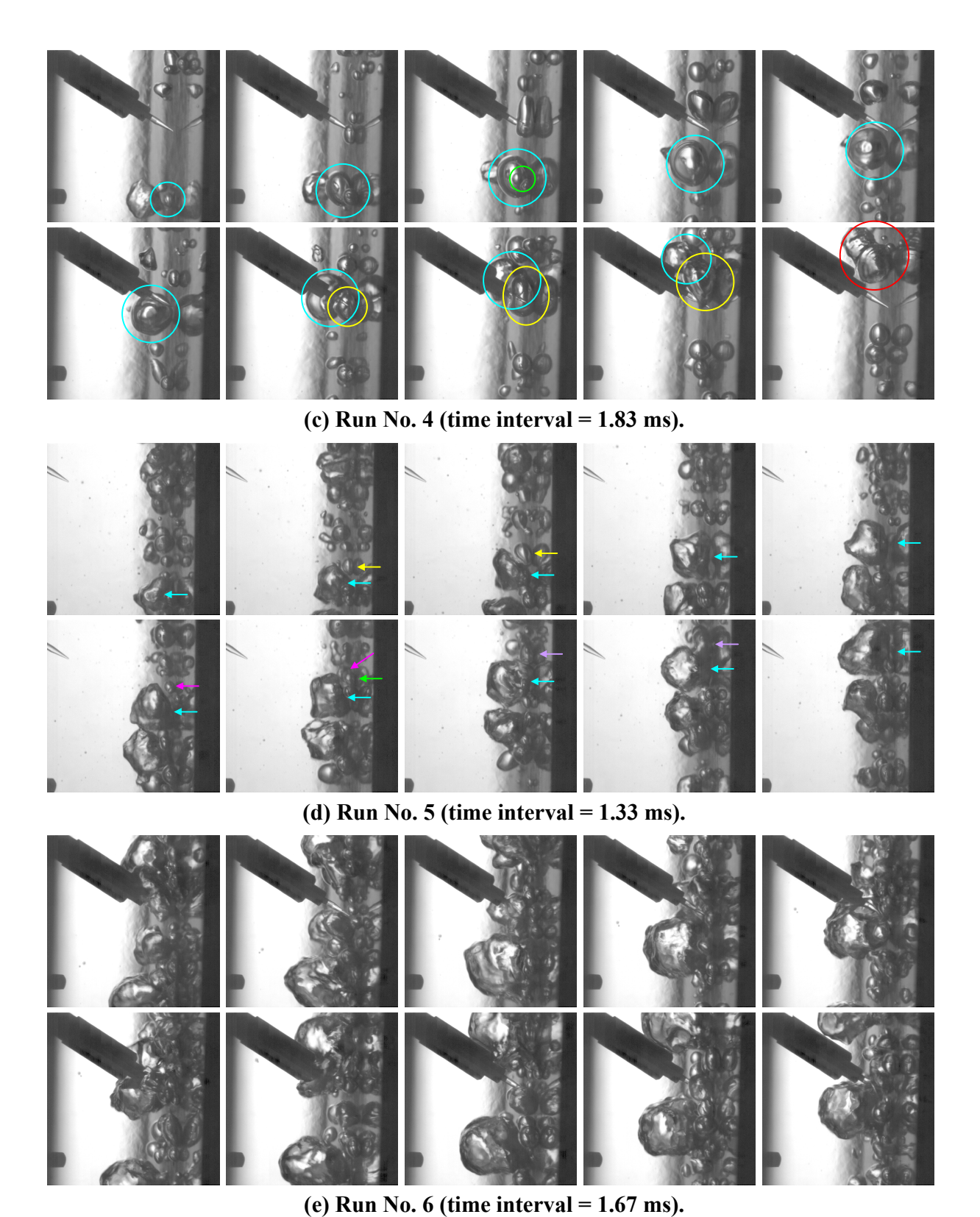


Figure 7 (Continued).

(9/11)

### 5. Conclusion

Bubble behavior in water subcooled flow boiling was studied to investigate the triggering mechanism of the net vapor generation under a low-pressure, low-flowrate and small contact angle condition. Bubble behavior observed in this work significantly depended upon the liquid subcooling. Under high subcooling conditions, bubbles were lifted off the wall immediately after the nucleation and collapsed in the subcooled bulk liquid. Since the condensation rate was nearly equal to the vaporization rate, an increase in the vapor void fraction with an increase in the thermal-equilibrium quality was small. Under sufficiently low subcooling conditions, bubble coalescence led to a formation of large sliding bubbles. The life-time of the sliding bubbles was long since they stayed in the high-temperature region adjacent to the wall. Furthermore, the sliding bubbles repeated the coalescence with other small bubbles to prevent the unidirectional migration of the small bubbles away from the wall. The possibility that the large sliding bubbles contributed to the enhancement of vaporization was also indicated. It is considered that the bubble coalescence followed by the formation of large sliding bubbles plays an important role in initiating a rapid increase in the vapor void fraction with an increase in the thermal-equilibrium vapor quality under the experimental condition tested in the present work.

# 6. References

- [1] M. Aoyama, K. Haikawa, L. E. Fennern, R. Yoshioka, T. Ohta, T. Anegawa, Optimization of core design for the next generation BWR, Proceedings of the 5th International Conference on Nuclear Engineering, Nice, France, 1997, Paper No. 2636.
- [2] M. Chaki, M. Murase, Evaluation of the sensitivity of a two-phase flow model for steam separators analysis, Proceedings of the 14th International Conference on Nuclear Engineering, Miami, Florida, 2006, Paper No. 89507.
- [3] J. G. M. Andersen, J. L. Casillas, B. S. Shiralkar, Application of advanced thermal hydraulic TRACG model to preserve operating margins in BWRs at extended power uprate conditions, Proceedings of the International Congress on Advances in Nuclear Power Plants, Reno, Nevada, 2006, pp. 1066–1077.
- [4] K. Arai, A. Murase, R. Hamazaki, M. Kuroki, AB1600-progress of ABWR technology toward next generation ABWR, Nuclear Engineering and Design, Vol. 238, 2008, pp. 1902–1908.
- [5] J. G. Collier, J. R. Thome, Convective boiling and condensation (3rd edition), Oxford University Press, Oxford, 1994.
- [6] P. G. Kroeger, N. Zuber, An analysis of the effects of various parameters on the average void fractions in subcooled boiling, International Journal of Heat and Mass Transfer, Vol. 11, 1968, pp. 211–233.
- [7] P. Saha, N. Zuber, Point of net vapor generation and vapor void fraction in subcooled boiling, Proceedings of the 5th Heat Transfer Conference, Tokyo, Japan, 1974, pp. 175–179.

- [8] N. Basu, G. R. Warrier, V. K. Dhir, Wall heat flux partitioning during subcooled flow boiling: part 1-model development, Journal of Heat Transfer, Vol. 127, 2005, pp. 131–140.
- [9] S. Levy, Forced convection subcooled boiling-prediction of vapor volumetric fraction, International Journal of Heat and Mass Transfer, Vol. 10, 1967, pp. 951–965.
- [10] H. C. Ünal, Determination of the initial point of net vapor generation in flow boiling systems, International Journal of Heat and Mass Transfer, Vol. 18, 1975, pp. 1095–1099.
- [11] E. L. Bibeau, M. Salcudean, A study of bubble ebullition in forced-convective subcooled nucleate boiling at low pressures, International Journal of Heat and Mass Transfer, Vol. 37, 1994, pp. 2245–2259.
- [12] T. Okawa, T. Ishida, I. Kataoka, M. Mori, Bubble rise characteristics after the departure from a nucleation site in vertical upflow boiling of subcooled water, Nuclear Engineering and Design, Vol. 235, 2005, pp. 1149–1161.
- [13] Y. Hirose, T. Hayashi, T. Hazuku, T. Takamasa, T., Experimental study on contact angle of water droplet in high-temperature condition, Proceedings of the 14th International Conference on Nuclear Engineering, Miami, Florida, USA, 2006, Paper No. 89614.
- [14] T. Takamasa, T. Hazuku, K. Okamoto, L. Mishima, M. Furuya, Radiation induced surface activation on Leidenfrost and quenching phenomena, Experimental Thermal and Fluid Science, Vol. 29, 2005, pp. 267–274.
- [15] T. Okawa, T. Harada, Y. Kotsusa, Photographic study on bubble motion in subcooled pool boiling, Journal of Engineering for Gas Turbines and Power, Vol. 132, 2010, Paper No. 102922.